The guessing game

Analysis of cyclic loaded foundation as a finite state transition system

Sabaliauskas, Tomas; Ibsen, Lars Bo

Publication date:
2018

Document Version
Publisher's PDF, also known as Version of record

DEPARTMENT OF CIVIL ENGINEERING
AALBORG UNIVERSITY

The guessing game

Analysis of cyclic loaded foundation as a finite state transition system

Tomas Sabaliauskas
Lars Bo Ibsen

ISSN 1901-726X
DCE Technical Report No. 249

Aalborg University
Department of Civil Engineering
Group Name

DCE Technical Report No. 249

The guessing game

Analysis of cyclic loaded foundation as a finite state transition system

by

Tomas Sabaliauskas
Lars Bo Ibsen

October 2018

Scientific Publications at the Department of Civil Engineering

Technical Reports are published for timely dissemination of research results and scientific work carried out at the Department of Civil Engineering (DCE) at Aalborg University. This medium allows publication of more detailed explanations and results than typically allowed in scientific journals.

Technical Memoranda are produced to enable the preliminary dissemination of scientific work by the personnel of the DCE where such release is deemed to be appropriate. Documents of this kind may be incomplete or temporary versions of papers—or part of continuing work. This should be kept in mind when references are given to publications of this kind.

Contract Reports are produced to report scientific work carried out under contract. Publications of this kind contain confidential matter and are reserved for the sponsors and the DCE. Therefore, Contract Reports are generally not available for public circulation.

Lecture Notes contain material produced by the lecturers at the DCE for educational purposes. This may be scientific notes, lecture books, example problems or manuals for laboratory work, or computer programs developed at the DCE.

Theses are monograms or collections of papers published to report the scientific work carried out at the DCE to obtain a degree as either PhD or Doctor of Technology. The thesis is publicly available after the defence of the degree.

Latest News is published to enable rapid communication of information about scientific work carried out at the DCE. This includes the status of research projects, developments in the laboratories, information about collaborative work and recent research results.

Published 2018 by
Aalborg University
Department of Civil Engineering
Thomas Manns vej 23, 9200
Aalborg, Denmark

Printed in Aalborg at Aalborg University

ISSN 1901-726X
DCE Technical Report No. 249

Recent publications in the DCE Technical Report Series

The making of Andersen’s liquefaction chart
Sabaliauskas, T. & Ibsen, L. B.
2017, DCE Technical Memorandum; No. 62.

Obtaining the Andersen's chart, triangulation algorithm
Sabaliauskas, T. & Ibsen, L. B.
2016, DCE Technical Memorandum; No. 53.

1 Introduction

Episodic loss and recovery of stiffness is observed in full-scale offshore foundations [12], [3]. This phenomenon is especially relevant to offshore wind turbines, as the slender structures rely on foundation stiffness to avoid resonating with cyclic loads. Unfortunately, dynamic loaded sand response (and therefore foundation response) is not well understood [4]. Sand has notoriously non-linear, counter intuitive properties, which arise from the very nature of this material: sand is made of individual grains. The grains re-arrange and re-interlock, forming complex networks of force chains [19], [2]. Each time sand is deformed, the soil fabric is disturbed permanently: the grains physically rotate and move to a new arrangement. Consequently, the same loads generate different outcomes, depending on how the grains are arranged (as shown in Fig.1).

There are infinite number of unique grain arrangements (soil states S). If the same action of testing (At) is applied starting at different arrangement S, each S generates a unique stiffness path $\pi(S, At)$ (see Fig.1). However, some $\pi(S, At)$ look similar. Therefore, can be grouped together: if $\pi(S1, At) \approx \pi(S3, At)$, then $S1 \approx S3$. The opposite is also true: if $\pi(S1, At) \not\approx \pi(S2, At)$, then $S1 \not\approx S2$. Thus, similar (equivalent) soil states can be categorized relative to each other. This allows to discretize an infinite-state problem into a finite-state transition system. Based on this premise, a novel, original testing procedure was formulated.

The original testing procedure introduced here is called "the guessing game". The procedure begins with acknowledging that the "initial state" of soil is not known. This is the case for wind turbine foundations during a storm - the soil is repeatedly disturbed and stabilized, thus the "initial" state is not known. However, a test starting with unknown soil state $S*$ can be tested by some action of testing At. Thus, generating a reference stiffness path, a "signature" $\pi(S*, At)$. The signature serves as a reference, according to which $\pi(S*, At)$ can be categorized. If at some point the same stiffness path is generated by At, one can say the "initial stiffness path" was reset (meaning, the "initial state" was reset). Such is the ultimate goal of the guessing game - to find a path back to "initial stiffness path".

The guessing game maps soil states into a decision tree, where S are the nodes and A are the links. Sequences of actions preserved in A vectors cause transition from one soil state S to another. The decision tree grows by iterating through sequence $S *\overset{At}{\rightarrow} S\overset{A*}{\rightarrow}S*$. Each cycle has an inductive phase (reaching for unknown soil state $S*$ by guessing $A*$) and a deductive part (converting unknown $S*$ to known S through applying At to test for the signature). As the causal tree grows, knowledge is preserved: as $S*$ get converted to S, it becomes plausible to deterministically predict which S will be caused by action A. As the game progresses, sequences of actions within A vectors become shorter. When the decision tree converges, vectors A contain purified causation, which allows to move from S to S using the shortest route.

The guessing game was contemplated intuitively from exposure to philosophy of science and principles found in machine learning and computer engineering

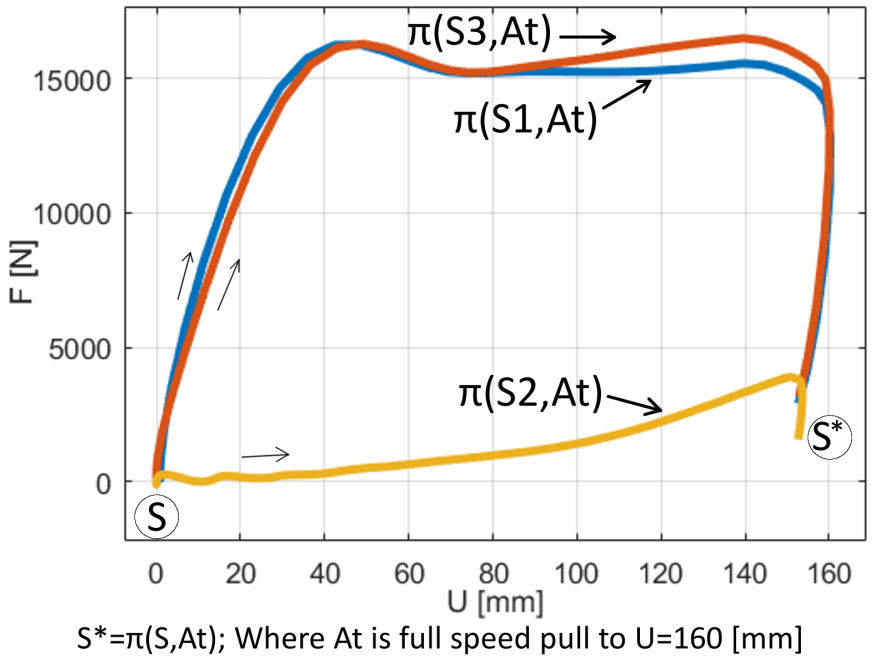

Figure 1: The same action generates different outcomes. Three different stiffness paths $\pi(S, At)$ were generated by the same action At. Different S was present before the At, thus each S, At combo leaves a unique "signature". If equivalent signatures are put into discrete categories ($S1 \approx S3; S2 \not\approx S3$), infinite-state is deduced to a finite-state problem.

(state-transition systems). The principle implements ideas inspired by work of Thomas Kuhn [1], where truth is described as both observable (inductively) and non-falsifiable (deductively). Inductive phase embraces "guessing" - extrapolating towards unknown soil states from a known one. Deductive phase embraces removal of irrelevant factors from A links (removing what's falsifiable). The case study presented in this paper uses the guessing game to analyze properties of a cyclic loaded foundation prototype embedded in sand. At first glance it may seem tempting to use conventional geotechnical models for "guessing", but convention collapses at a certain point: loading scenarios combining drained and undrained response during irregular loading cycles, reaching highly disturbed soil states, which are then reversed back to initial state - are beyond the scope of convention. Thus, convention is avoided. When guessing, $A*$ are intentionally randomized and scrambled to explore counter intuitive corners of the finite-state system. The problem is treated like a genuine state-space transition system. The user is given a joystick attached to a hydraulic piston pushing a foundation prototype back and forth. Then, the "player" is given the task to find a sequence of A which would re-generate the first stiffness path $\pi(S_o,\, At)$. Thus, essentially disturbing the foundation back to "initial" state. Decisions are made following intuition and real-time decision making, rather than a premeditated action sequence. The player is challenged to generate and test ad-hoc mental models and assumptions following real-time feedback from the object being tested.

2 Equipment

Aalborg University (AAU) geotechnical laboratory has a long history of R&D in geotechnical testing equipment. From frictionless triaxial and consolidation apparatuses [10], to sand boxes recreating water pressures found at the sea floor [14]. The sand boxes are used for testing the mono-bucket foundation - an innovative offshore wind turbine foundation, designed to compete with mono-piles. After decades of R&D, the mono-bucket has recently entered offshore wind turbine market. The patented concept is now represented by Universal foundation A/S. The mono-bucket uses less steel and is installed faster than a mono-pile. Also, installation of the mono-bucket is quiet, and it can be decommissioned without leaving a footprint (removed by reversing the suction pump, thus pushing the suction caisson out of the sea floor). Research of the mono-bucket is part of M.Sc. and Ph.D. theses at AAU. Consequently, a small scale mono-bucket was readily available for the case study presented in this paper. Schematics of the testing rig and the mono-bucket used are given in Fig.2 and Fig.3.

The testing rig (Fig.2) contains a sand box inside a pressure chamber. The pressure chamber allows to generate pore water pressures found at the sea floor. $200kP\,a$ pressure is used to imitate $20m$ water head. Pressurizing the water is important for undrained soil response, encountered during rapid (impact) loading. If sand is deformed fast, undrained response is generated. The pore water cannot escape, the volume of voids becomes "locked" by pore water stiffness.

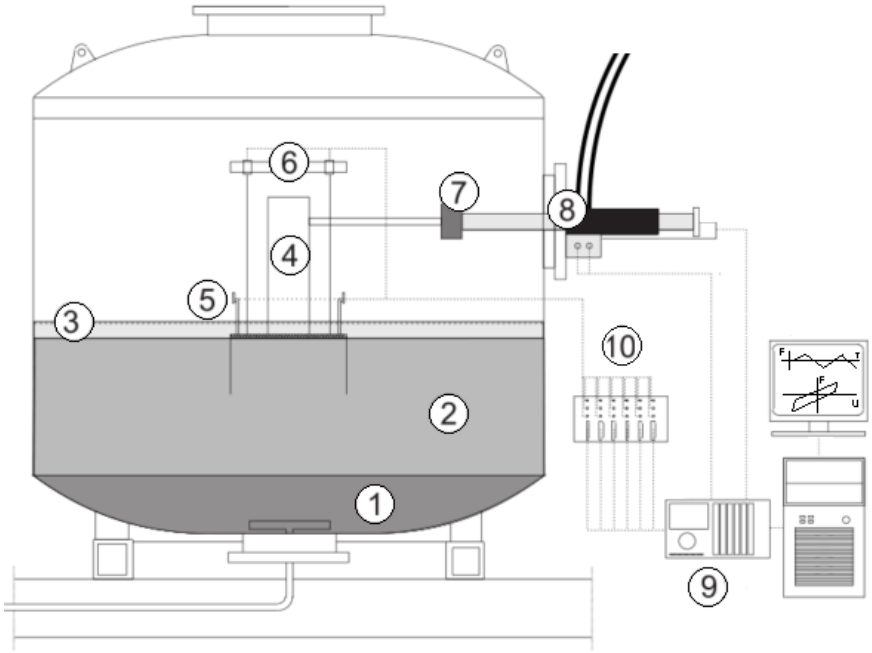

Figure 2: The testing-rig. A sand box within a pressure chamber, for small scale foundation testing. 1) Bottom layer of soil is gravel. It acts as a filter for drainage tubes. 2) Aalborg University sand No.1. 3) Water head above soil level. The soil is fully saturated at all times. 4) The monobucket, attached to a shaft. 5) Valves and warer pressure transducers, measuring water pressure along the skirt, and below the lid. 6) Displacement transducers. A total of three displacement are measured. 7) A load cell, measuring focre. 8) A high pressure, digital walve controolled piston. 9) MOOG controller / data logger, with automated load control and realt ime data plotting options. 10) MGC plus data acquisition box [13]

This makes dilative sand (and structures built in it) much stronger and resistant to impact loads [23], [13]. The benefit of increased peak strength is counter balanced by the potential of losing stiffness due to liquefaction. Especially during two-way cyclic loads [16], [17]). The additional undrained strength component is called "the boot effect" by some authors [14], because to pull a boot out of mud one has to pull slowly - fast loads generate additional pore water pressures, which add resistance. Interestingly, the case study presented here shows the boot effect is lost when stiffness is lost, and recovers when stiffness recovers. Thus, the boot effect is a "state dependent" phenomenon as well, pore pressure effects are part of the stiffness path generated during $\pi(S, At)$. Thus, if the initial soil state is recovered, the boot effect will recover with it. High water pore pressure amplifies the boot effect, thus the boot effect is especially relevant for deep water foundations [9].

In the testing rig (Fig:2) a mono-bucket prototype is inserted in sand. A simplified schematic of the test is given in Fig.3. The caison foundation has a large diameter lid, with a skirt along the periphery. The large diameter skirt provides large leverage, which makes skirt friction more efficient at resisting overturn moment. In addition, the lid provides a large surface for distributing the vertical load (static weight of a wind turbine). Thus, the mono bucket acts like a gravity foundation, distributing the vertical load across a large surface area, while the skirt is optimized to resist overturning. Together, the two components form a water tight caisson, which traps a large mass of soil and water. Thus adding mass for added stability.

As mentioned earlier, the mono-bucket is meant to rival mono-pile foundations. The purpose of the mono-bucket is to improve current offshore industry standard for intermediate water depth offshore foundations. The mono-bucket is lighter in weight, faster to install [11]. The mono-bucket can also be quickly and cheaply un-installed, without leaving a footprint. In addition, there is no need for scour protection, as the lid itself protects against scour [20]. Thus, the mono-bucket has the advantages of cheaper production, faster installation, easy decommission, and no added costs associated with noise mitigation or scour protection. Despite all the benefits, the mono-bucket is a novel concept, which brings higher risk factors. Potential clients are cautious of novelty largely because dynamic loaded sand properties are not well understood [4], and the mono bucket provokes a complex array of phenomenon combining drained, undrained and partially drained soil response. Thus, tests researching the dynamic properties continue, and the new approach (the guessing game) is attempted to gain new knowledge. The prototype in Fig.3 is 500 mm in diameter, and 500 mm in height. The skirt is 6 mm thick. There is one, horizontal hydraulic piston attached at the top of the shaft (the shaft is approximately 300mm long). The hydraulic piston if controlled by proportional-integral-derivative (PID) controller, with a load cell and a displacement transducer attached to the piston.

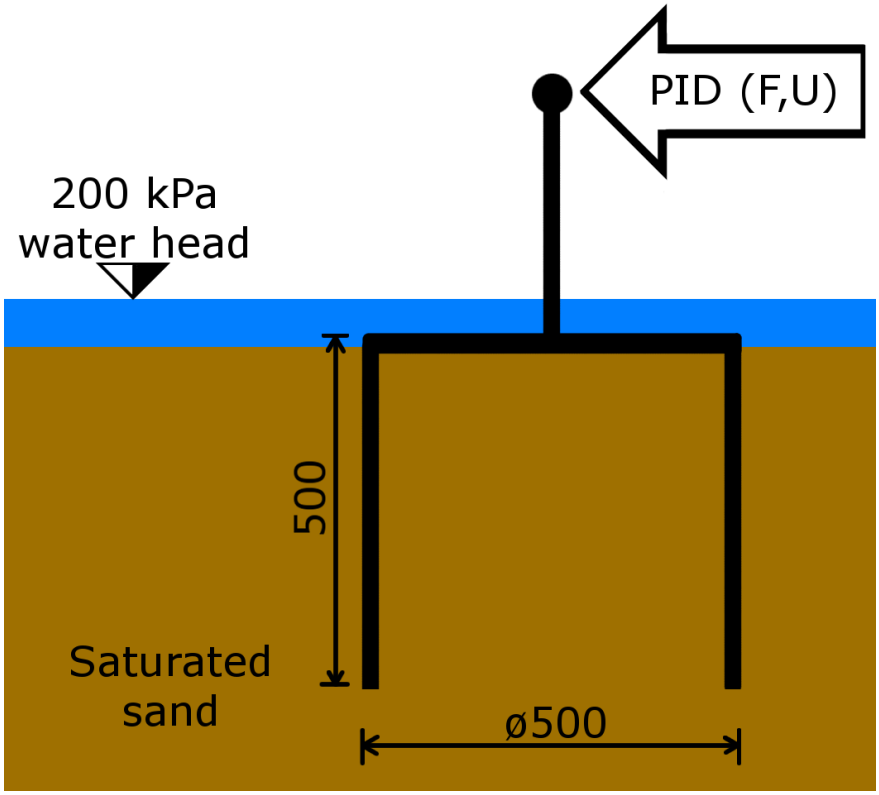

Figure 3: The small scale mono bucket foundation is inserted in fully saturated sand. Either force or displacement can be applied horizontally on the top tip of the shaft. The testing rig is placed within a pressurized chamber, where 200 kPa pressure is applied to imitate 20 m water depth. The extra pore pressure is important for increasing dynamic peak strength [13], [23], [8]

.

3 Methods

The testing equipment is rather simple - a hydraulic piston pushing / pulling a foundation at the top of the shaft. The hydraulic piston applies the inputs, the foundation generates outputs. The equipment is simple in construction, but the foundation prototype generates complex, nonlinear, state-dependent outputs. To make analysis manageable, the problem is reduced to a minimum number of variables - stiffness is observed by monitoring force (F) and displacement (U) at the tip of the shaft (see Fig.3). In this study U is used as the input, F is measured as the output.

U is used as the input because "we can always map to load from displacement, but not always from load to displacement" - David Muir Wood lecture, 2015. Using F for input imposes significant limitations. Firstly, F inputs are only conditionally stable: given F beyond the peak strength U accelerates towards infinite, causing loss of control and endangering the testing equipment. F cycles are plausible to apply only within the limits of peak strength. Secondly, even within confines of peak strength limits, F inputs provoke a combination of nonlinear stiffness (K), damping (C) and inertia (M) forces (see equation of motion, Eq.1). Thus, applying F provokes three nonlinear components - state dependent $K \cdot U$, state dependent $C \cdot \frac{\delta U}{\delta t}$, and state dependent $M \cdot \frac{\delta^2 U}{\delta t^2}$. This means that, whenever F is applied as the input, the output is encrypted under three layers of nonlinear state functions. Which is very hard to decipher, as the equation $K = U^{-1} \cdot [F - \frac{\delta U}{\delta t} \cdot C - \frac{\delta^2 U}{\delta t^2} \cdot M]$ would have to be solved, while all three: K, C and M are unknowns.

$$F = K \cdot U + C \cdot \frac{\delta U}{\delta t} + M \cdot \frac{\delta^2 U}{\delta t^2}. \tag{1}$$

On the other hand, when U is the input, it is applied wile controlling $\frac{\delta U}{\delta t}$ and $\frac{\delta^2 U}{\delta t^2}$. Therefore, attempts can be made to find loading setting where $\frac{\delta U}{\delta t} \to 0$, thus making $C \cdot \frac{\delta U}{\delta t} \approx 0$. Also $\frac{\delta U}{\delta t}$ input can be varied very slowly, making $\frac{\delta^2 U}{\delta t^2} \approx 0$. Thus, allowing to cancel two out of three components in equation of motion, consequently isolating $F = U \cdot K$. This allows to analyze state dependencies of quasi-static $K = \frac{F}{U}$. If (in the future) phenomenon governing K are fully understood, then the loading rate could be increased to where $C \cdot \frac{\delta U}{\delta t} \not\approx 0$, and the effects of C could be isolated by solving $C = \frac{\delta t}{\delta U}[F - K \cdot U]$. Alas, rules governing quasi static K must be discovered beforehand. Nevertheless, using U as the input has the potential to observe one nonlinear (state dependent) component at a time, and potentially decode the entire nonlinear, state dependent equation of motion.

For reasons given, U is defined as the input. The F is plotted (and analyzed) as a function of U (the foundation is treated as an $F(U)$ system). Analysis of resulting data plots is conducted purely graphically: measured data is plotted, stiffness paths $\pi(S, At)$ are visually inspected, and the player makes real time judgment based on charts plotted on the computer screen, during real-life, real-time testing. The goal is to recover the "initial" stiffness path $\pi(S_o, At)$.

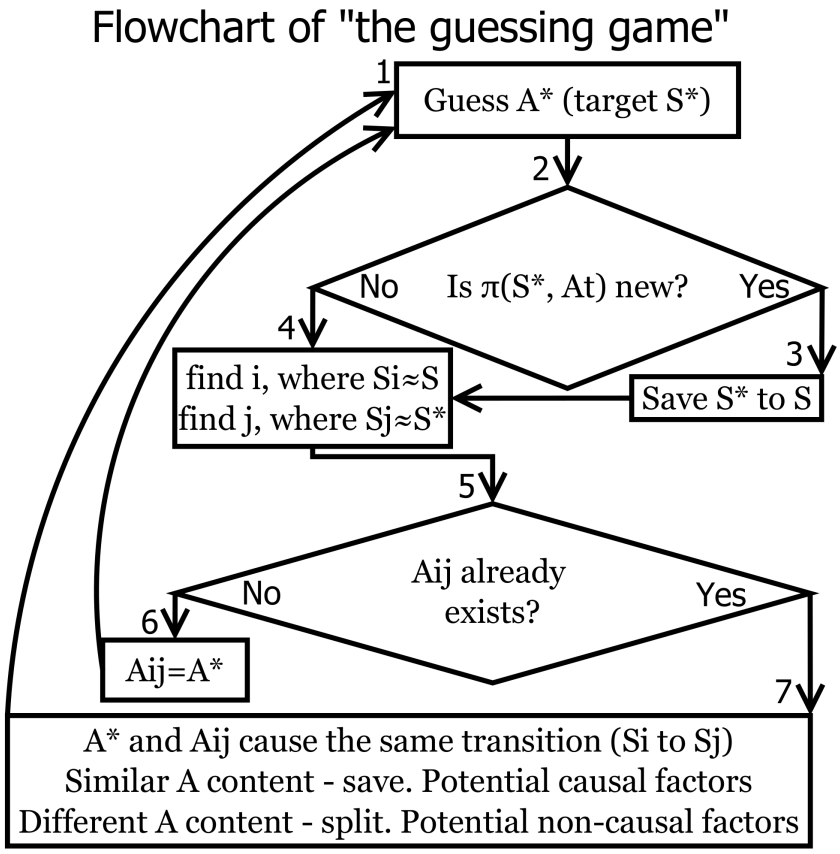

Figure 4: The three stages of "the guessing game". Detecting new nodes, detecting links, detecting conflicts between guessed and known links.

Because the method to reset the initial state are not known, the researcher has to begin the procedure by blindly guessing the action sequence $A*$, Then, after $A*$ is applied, consequent state $S*$ is tested using At, and the guessing game continues. Once a sequence A leading to S_o is found, the game can continue to improve efficiency of the solution by looking for causal factors within the A sequence. The game ends when the causal factors governing cyclic foundation stiffness are found - the optimal path to S_o is found.

As mentioned in the introduction, the guessing game draws a causation tree, a type of a flowchart. Links are inductively guessed and deductively trimmed. In the process, a finite set of data structures can be encountered. To illustrate them, the links and nodes are divided into subcategories: four types of links, and two types of nodes (see Table.1).

1. Nodes - the consequences of applying A.
   (a) Known (S). States with known signatures, tested by At (marked as $S^{\overrightarrow{At}}$ in diagram Fig.5).
   (b) Predictor (S^*). States with unknown signatures, before applying At.
2. Links (sequence of actions) - the causes of changing S.
   (a) Predictor (A^*). Scrambled, randomized, guessed action sequence with unknown outcome, creating $S*$.
   (b) Transition (A_{ij}). Action sequence known to cause transition from S_i to S_j.
   (c) Self reference (A_{ii}). Action sequence preserving the same S after testing.
   (d) Causal action (Aj). Action which causes Si to occur regardless what S the Aj is applied from.

Table 1: Types of nodes and links encountered during the guessing game.

Known node (S): In a deterministic finite-state system, pairs of S are connected with one unique A. Thus each $\pi(S, A)$ has unique outcomes. If applying the same A sequence generates different $\pi(S, A)$, the cause can only be attributed to difference in S.

Predictor node ($S*$): States with unknown $\pi(S*, At)$. The $S*$ can be generated in two ways - by interpolating or extrapolating. Interpolation is plausible, because S changes gradually. Soil grains do not "teleport" from one arrangement to another. Thus, if a known sequence A is paused before completion, the transition $S_i \overrightarrow{^{A_{ij}}} S_j$ is split into $S_i \overrightarrow{^{A_{ik}}} S_k^* \overrightarrow{^{A_{kj}}} S_j$. Thus, S_k^* is predicted (interpolated) between two known states. Similarly, S^* can be extrapolated, by starting from a known S and applying a sequence which has not been applied there: $S^{\overrightarrow{A*}} S*$, where S is known, but the action A^* had never been applied starting at S. Thus, extrapolating into unknown.

Predictor link (A^*): When actions $A*$ are applied for the first time, the consequent $S*$ is unknown. It is not known what $S*$ is created by $A*$ until the signature $\pi(S*, At)$ is tested. The uncertain outcome means $A*$ can either detect a new link, or cause a conflict with already known A_{ij}. (see Fig.5-a,b)

Transition link (A_{ij}): Actions causing transition from S_i to S_j. Only one A_{ij} can be defined between S_i and S_j. When A_{ij} is observed for the first time, the action sequence will not be optimal. As the game continues, $A*$ will start to conflict with existing A_{ij}, causing the same transition to occur using two

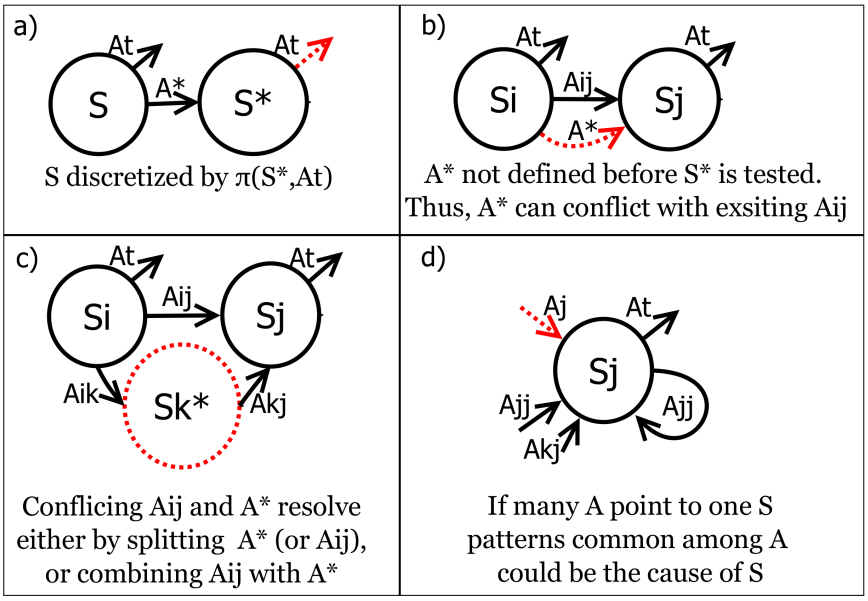

Figure 5: Key data structures observed during "the guessing game".

different paths (see Fig.5,b). The conflict can be resolved in 2 ways: either by splitting A_{ij} and introducing a new node S_k* (Fig.5,c), or combining the conflicting A_{ij} and $A*$ deductively (Fig.5,d). Similarities between conflicting $A*$ and A_{ij} are potential causal factors. Transition from S_i to S_j is causal, thus if $A*$ and A_{ij} have similarities - those are likely to be a causal factor. Differences in conflicting A_{ij} and $A*$ are non-causal factors, which allows to deductively trim the sequence saved in A_{ij}.

Self reference link (A_{ii}) A special case of A_{ij} is when $i = j$. This means the S_i was either not disturbed at all by actions in Aii, or the Si was both disturbed and reversed during the sequence A_{ii}. The correct case can be diagnosed by splitting $A_{ii} = A_{ij} + A_{ji}$, and interpolating $S*$. In data plots, such structures generate self overlapping hysteresis loops. These are very interesting, as they provide an observable reference point which can be detected without applying At. Thus, self overlapping hysteresis loops can serve as a local convergence point, which helps the user to orient within the decision tree without using At.

Causal link (A_j) A special case of A_{ii} is A_j, which can be deduced after multiple A are noticed to point towards one S (Fig.5,d). If Sj has a cause, and the cause is purified, then regardless what S or $S*$ the A_j is applied from, the outcome is always Sj. This case can be written as $Sj = \pi(S*, Aj)$. The objective of the entire game can be defined as looking for Ao, as Ao is the action guaranteed to recover So - the initial stiffness path $\pi(So, At)$. This is

only plausible if Ao contains the causal factor governing the "initial state". Thus, by analyzing Ao, the cause could be extracted and implemented in a physical model of the system being analyzed.

When implemented, the subcategories of nodes S and links A allow to propagate knowledge through the causal tree - known sequence At allows to convert unknown $S*$ into known S. Known S are used to convert unknown $A*$ into known A_{ij}. Known A_{ij} start conflicting with $A*$. Through deductive resolve, A_{ij} are trimmed down to A_j, and finally Ao. It is remarkable "knowns" can be used to define "unknowns".

4 Results

While playing the guessing game, a phenomenon was discovered. The phenomenon of converging stiffness hysteresis loops. When deformation cycles of amplitude $Umob$ are applied at the tip of the foundation prototype, stiffness hysteresis loops converge to a stable contour (see Fig's. 6, 7). This means the soil structure goes through a sequence of equivalent S states, in a closed loop. A sequence of S becomes locked in a phase dependent, temporally "stable state". In state transition diagram, this is a self referencing structure $S_i \xrightarrow{A_{ii}} S_i$ (see Fig.5).

It is interesting to analyze the phenomenon in more detail. The stiffness hysteresis loops shaped during $\pi(S, Umob)$ converge towards the same $Fmob$ amplitude. Every hysteresis loop is parametrized by unique $Umob$, but they all share the same $Fmob$ limits. If $Umob$ amplitude is made smaller (see Fig.6), the $Fmob$ limits graduall converge towards a hysteresis loop within the "min" and "max" limits. Similarly, if $Umob$ amplitude is increased (see Fig.7), the $Fmob$ gradually adapts as well. In both cases, the same F limits are followed, but given smaller $Umob$ amplitude the hysteresis loop is steeper (higher stiffness), while larger $Umob$ amplitude creates a hysteresis loop stretched across a larger deformation amplitude, thus stiffness is lower. This reveals an interesting feature of the system: it is not plausible to tell which stable state is currently active, by looking at $Fmob$ amplitude (all stable hysteresis loops share the same F limits), but each stable state can be uniquely described, predicted and controlled by $Umob$ (stiffness hysteresis loops are uniquely dependent on $Umob$ amplitude). Thus, it is not plausible to predict which hysteresis loop is active by observing F amplitude. The hysteresis loops can be uniquely described, predicted and prescribed only by observing / controlling the $Umob$ parameter.

The observed $Fmob$ and $Umob$ relationship allows to deduce a causal pattern: all $Umob$ converge towards one $Fmob$ (given a constant loading frequency, 0.1 Hz in this case). Thus, $Fmob$ can be efficiently expressed as a function of $Umob$. However, the opposite is not true, $Umob$ cannot be defined as a function of $Fmob$, as one $Fmob$ is shared by infinite $Umob$. This makes sense given the fact that deformation is essential for soil grains to rearrange (soil state S to change). Stress cycles can be applied without moving the grains. Whereas deformation forces the grains to move, rotate and re-arrange. If the force is

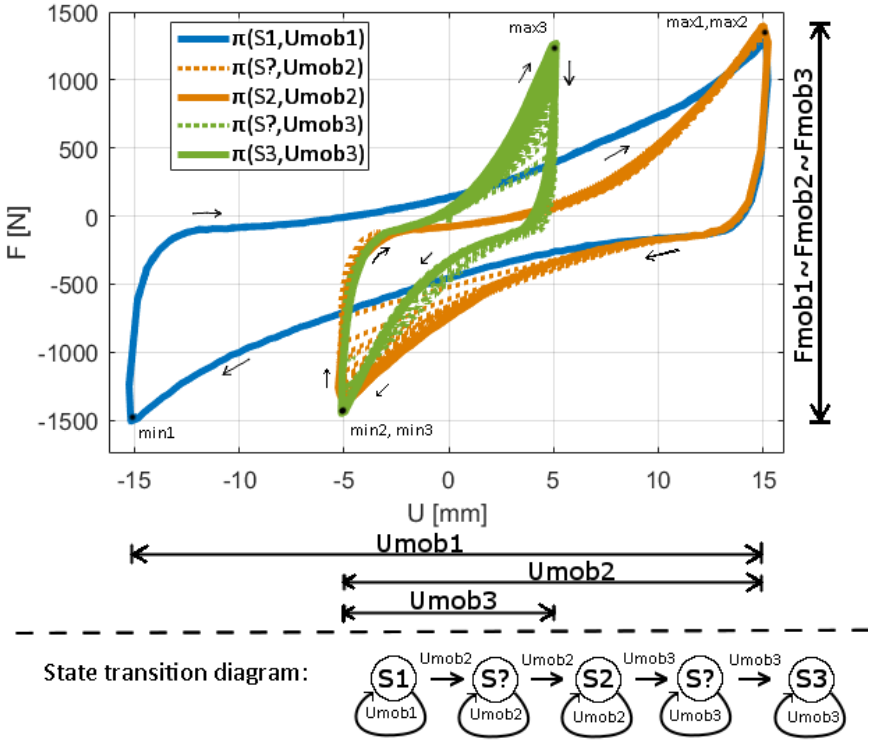

Figure 6: Deformation cycles transitioning from bigger to smaller $Umob$. Notice, all $Umob$ converge to similar $Fmob$ amplitudes.

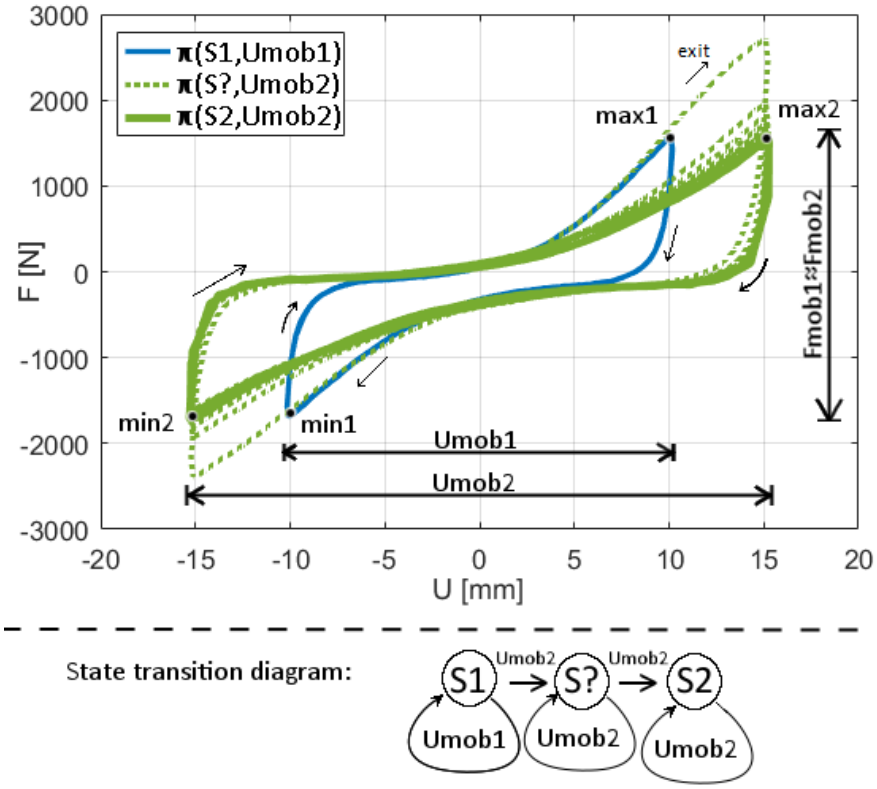

Figure 7: Deformation cycles transitioning from smaller to bigger $Umob$. Notice, both $Umob$ converge to similar $Fmob$. Upon exiting $Umob1$, the tangent stiffness path shoots above the $max1$. But F at $max2$ stabilizes equivalent to F at $max1$.

removed, but deformation is applied - soil state changes. Whereas, locking the grains together (removing the deformation) and applying the stress cycles would not change the soil state.

During each deformation cycles, infinite different S are transitioned, as the transition is gradual - grains do not "teleport" from one arrangement to another. (sequence A_{ii})), the S being transitioned overlap in phase with equivalent S sequence generated during the previous loading cycle. Thus equivalent S re-occur in phase with the deformation cycle. A temporal "stable state" is reached, the phase dependent S pattern becomes synchronized, "locked" in a temporal loop (note, the hysteresis loops in Fig's 7 and 6 were generated at 0.1Hz frequency).

When exiting the stable state, the exit path follows a tangent trajectory. This is visible in Fig.7 while exiting point $max1$. This indicates that stable states generated at smaller $Umob$ will have a steeper exit path. To test this hypothesis, three stable states were generated at different $Umob$ amplitudes. The stable states were paused at the same deformation phase, to generate comparable exit paths. The result is shown in Fig.8. As expected, the smaller the $Umob$ the steeper the exit path (dynamic stiffness, combining K and C component from equation of motion).

At this point some causal assumptions can be made - if the "exit" stiffness path depends on the phase and diameter of $Umob$, then the initial stiffness path could be recovered by applying gradually smaller $Umob$, until the "initial" stiffness fully recovers. This assumption was tested, and the result is plotted in Fig.9. To evaluate success of stiffness recovery, stiffness paths generated using the new hypothesis are compared with pre-existing research of mono-bucket foundation. The "original" path is borrowed from preexisting research [14], [13].

In Fig.9 the "original" stiffness path was generated by following a labor intensive procedure, where the foundation prototype is removed using a crane, then water is allowed to rise from below the sand - producing an upward seepage gradient which loosens the soil. Then the soil is vibrated using an industrial vibrator and CPT tested in different spots of the testing rig to check if CPT results are consistent. The foundation prototype is then pushed back into the sand, cyclic loaded with small force amplitudes to emulate stabilization caused by small loading cycles prior to a storm. And then the At action is applied. Thus, "the original" stiffness path takes 2 days of preparation to execute one At test lasting just a few seconds.

Two days of preparation for a two second test is not very efficient. Worse yet, the "original" preparation method is both heavy manual labor and struggles to repeat the exact initial state So (manual labor brings human errors). The state transition analysis reveals a novel way to reset the initial state So - by applying gradually smaller $Umob$ amplitudes. Using the new method, At is applied starting with soil states $S1$ to $S5$ in Fig.9. Soil states $S1$ to $S5$ can be renamed to So, as they generate stiffness paths comparable with the "original", thus effectively "reseting" the stiffness path within minutes of each other. this allows to repeat the peak strength test 5 times in less than one hour.

If small $Umob$ cycles are not applied, the path $\pi((S5, At), At, At)$ in Fig.9

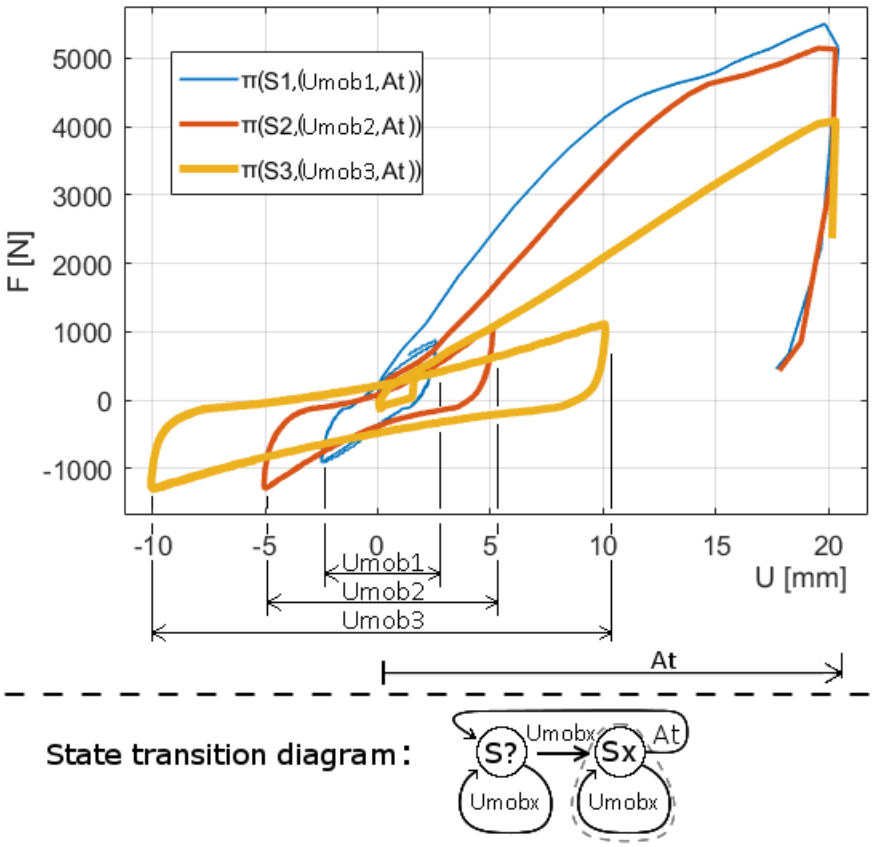

Figure 8: Three exit paths, measured after stabilizing three different stable states, at three different $Umob$. Note, At amplitude here is reduced to 20 mm. The state transition diagram is deduced to represent the general case.

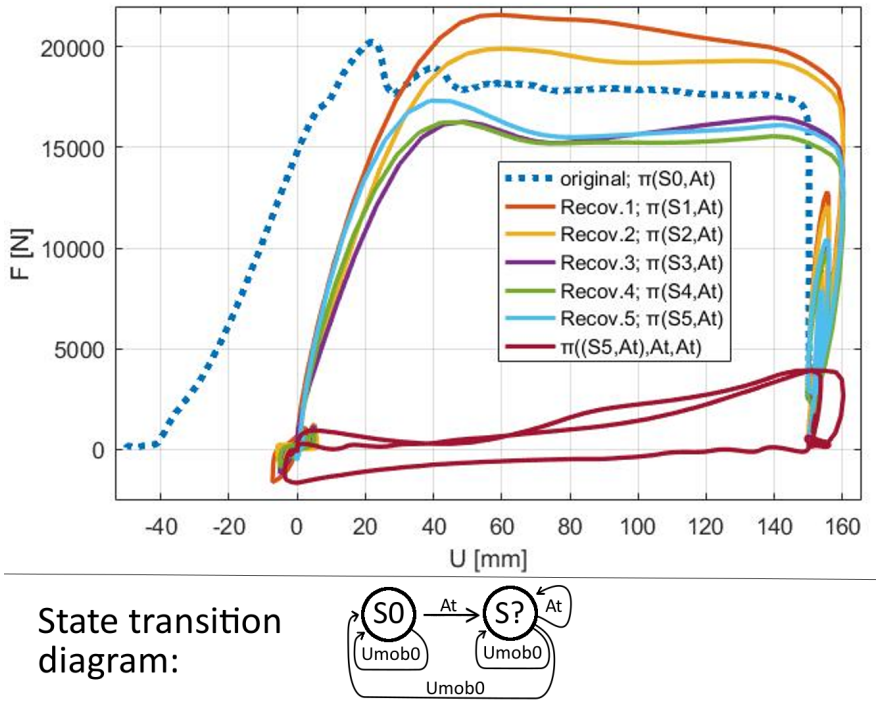

Figure 9: A test showing recovery of initial stiffness path (thus initial soil state So). The initial stiffness path was recovered 5 times in one loading history. Test result is compared with the "original" stiffness path published in preceding research [13].

is generated. $\pi((S5, At), At, At)$ is the "disturbed" stiffness path left after At. After At foundation stiffness drops very significantly. Interestingly, if At is applied multiple times in a row, if creates a temporal stable hysteresis loop at a large deformation amplitude. Only after stabilizing the hysteresis loop towards a small $Umob$ amplitude, the initial stiffness path is recovered. The observations is very simple, but it reveals an important physical property governing stiffness of a foundation embedded in sand - stiffness behaves as functions of deformation.

The stable states shown thus far were all generated at $\omega = 0.1Hz$ deformation frequency (using triangular sawtooth wave as U input). The triangular sawtooth wave has a constant $\frac{\delta U}{\delta t}$ between the peaks. Thus, when $\omega \to 0Hz$, then $\frac{\delta U}{\delta t} \to 0$. In methodology section, U was declared as input for this very reason: deformation can be applied slow enough to cause $\frac{\delta U}{\delta t} \approx 0$, thus canceling $C \cdot \frac{\delta U}{\delta t}$ effects. If true, there should be a loading rate where quasi static K is detected. Once $\frac{\delta U}{\delta t} \approx 0$, further reduction of $\frac{\delta U}{\delta t}$ will not produce detectable changes in stable state K stiffness hysteresis loop. The test shown in Fig.10 was run to test this assumption.

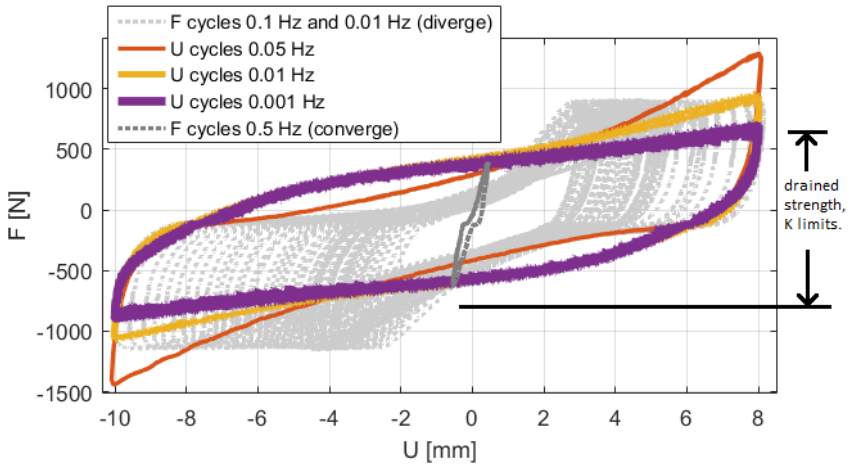

Figure 10: Stable state stiffness hysteresis loops, generated at varying loading frequencies. triangular sawtooth wave creates constant $\frac{\delta U}{\delta t}$ when U is the input. When F amplitude is input, $\frac{\delta U}{\delta t}$ is not controlled, hence C dependent deviation from static K is amplified.

As expected, slowing down ω causes converging changes within the hysteresis loop generated at a fixed amplitude. Pore pressure has more time to dissipate, thus deviation from quasi static K loop gradually diminishes. The K hysteresis loop observed at $\omega = 0.001Hz$ has no detectable C effects, and further reduction in ω does not produce further change. Because deviation from quasi-static loop depends on deformation rate, it can be attributed to the C component in equation of motion (Eq.1). Exposed to deformation, sand expands and contracts - the faster the volume change, the bigger the pore water pressure gradient. Thus, the C component can be attributed to pore water pressure gradients. If load is applied slow enough, then even tiny pore pressure gradients have enough time to dissipate - drained more. Therefore, the quasi-static stable state K loop can be viewed as purely drained soil response (in this case, at $\omega \leq 0.001Hz$).

The drained quasi static K stiffness path is very interesting, as drained response is effectively the back bone of soil fabric. When sand dilates or contracts, pore pressure varies and pushes the stress path above or below the drained path [17], [18]. Comparing the stiffness paths in Fig.10 it is visible that hysteresis loops have both contraction and dilation dominant loading phase. Stiffness loop drop below the drained path can be attributed to contraction dominant phase (partial liquefaction, loss of stiffness). The stiffness path above the drained hysteresis loop can be attributed to dilation (boot effect, increase in peak strength). Thus, giving valuable insights how state dependent K and C function coexist, and can be isolated from each other.

Finally, the drained stiffness hysteresis loop provides valuable reference points for cases where F is used for input (see Fig.10). F cycles within the drained

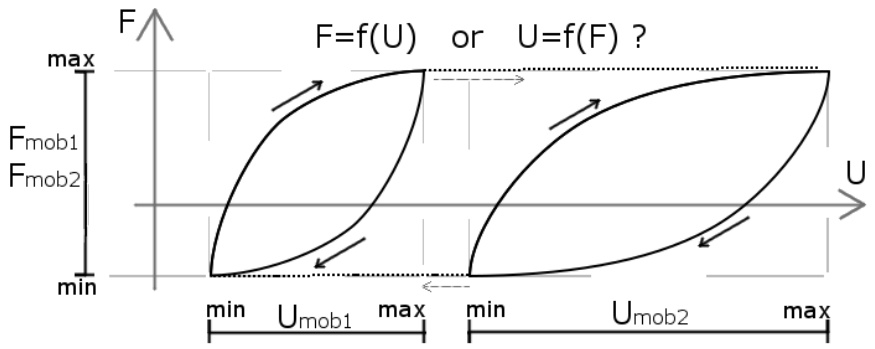

Figure 11: A thought experiment, illustrating the observed stiffness hysteresis loop behavior. Only $Fmob$ can be uniquely defined by $Umob$, therefore it is an $F = f(U)$ problem.

K limits converge towards $Umob \approx 1mm$. Thus, there is a $Umob$ amplitude towards which $Fmob$ cycles converge, regardless of relatively fast deformation frequency ($0.5Hz$ in Fig.10). On the other hand, F cycles reaching beyond the drained K loop limits are not stable. When F cycles exceed the drained limits, $Umob$ diverges towards infinite. Curiously, slower loading frequency creates larger deformation increments. This makes sense, given the C component acts as a linear damper - the more time is spent beyond the drained limits, the more time there is for deformation to accumulate. F beyond drained limits relies on pore water "locking" the voids at constant volume (resisting deformation). Because the system is partially drained, slow loading frequencies provide more time for water seepage, therefore allowing more water to fill the voids, thus more deformation - required for soil grains to change arrangement. Finally, notice how the stiffness hysteresis loops generated by $Fmob$ are notably more curved than those shaped during $Umob$ cycles. This is because $\frac{\delta U}{\delta t}$ is not limited by while $Fmob$ is applied. Therefore, at times of low stiffness, large $\frac{\delta U}{\delta t}$ accumulates, thus amplifying the $C \cdot \frac{\delta U}{\delta t}$ component, thus amplifying the curvature.

5 Discussion

In engineering practice, loads are collected and applied as F vectors. Engineers need to prevent excess inclination of a structure, thus it is tempting to look for $U(F)$ solutions, where deformation is predicted as a function of F history. However, the foundation behaves as an $F(U)$ system (see Fig.11). The F history can be uniquely described, predicted and prescribed as a funtion of U. Solutions using $F(U)$ models could have fundamental limitations when applied to $U(F)$ problems. The new experimental evidence suggests that, there is no unique $Umob$ for every $Fmob$, only a unique $Fmob$ for every $Umob$. Thus, $Fmob$ is uniquely predictable as a function of $Umob$, but not the other way round.

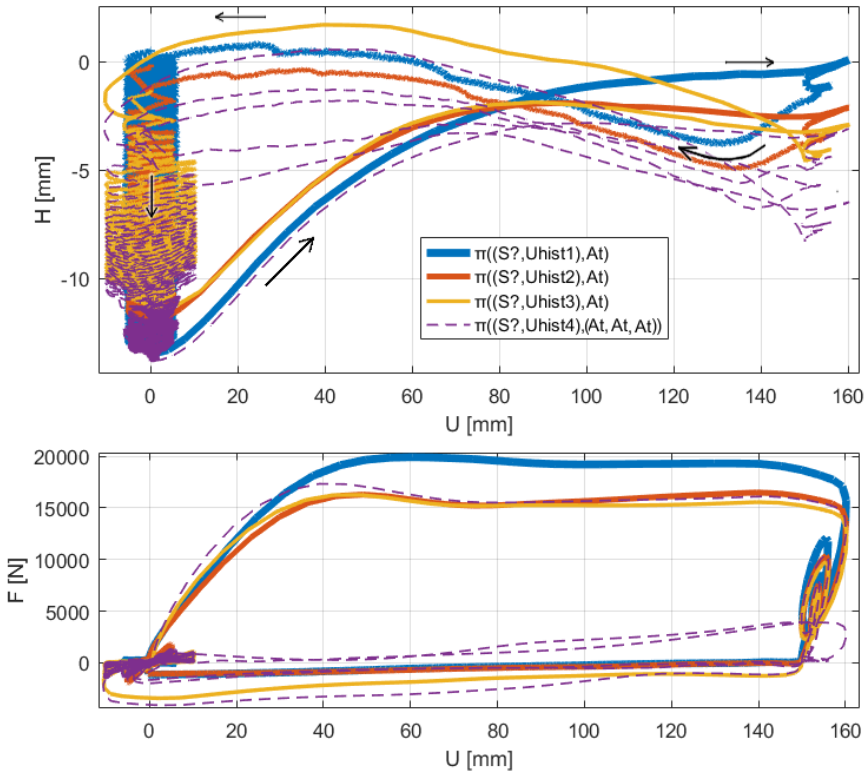

Figure 12: Loss and recovery of stiffness, is noticed to occur together with loss and recovery of foundation depth. Note the foundation has a flat, solid lid, thus the change in depth can occur only if the soil volume is contracting during stabilization, and dilating while being disturbed.

Stable state hysteresis loops preserve their overall shape by stretching and squeezed within $Umob$ amplitude. This type of behavior can be modeled by normalizing the stiffness path within a deformation envelope. Just like stress (or force) envelopes, deformation (or strain) envelopes can be used in modeling. A potential constitutive formulation for strain-space plasticity is readily available [22]. Strain-space formulation is interesting not only for its new found comparability with the new found experimental evidence. Strain-space plasticity has substantial computation benefits as well: fewer matrix inversions, reduced return mapping computation cost. There are ample examples of strain-space (stress relaxation) models in non-geotechnical paradigms of material science: cracking concrete [7], bone fractures [15] and aeronautic aluminum [22] had been successfully modeled by using strain-space (stress relaxation) envelopes. Thus, principles of strain-space plasticity could be borrowed from neighboring branches of material science.

Stiffness is the primary objective in this paper. But during the tests, the mono-bucket prototype was equipped with additional sensors not required for measuring stiffness. For instance, the vertical displacement of the bucket was measured as well (see plots in Fig.12). It is interesting to side note, that each time initial stiffness was recovered, the foundation was noticed to lower itself down, towards a repeatable depth. The wide lid of a mono bucket means the soil under the lid was compacting. Whereas, during peak strength test - the foundation raised itself upward (the soil volume dilated). Thus, the deformation cycles which produced stable state stiffness loops, produced stable state volumetric response as well. It is already known that liquefaction charts are best normalized by deformation (strain) amplitude [5], [6], and increasingly mode deformation dependent sand properties are being discovered in dynamic frictionless triaxial tests as well [17], [18]. Thus, there symptoms that deformation dependent properties of sand is an intriguing topic ripe with opportunities for pioneering research. To access these soil properties: new testing protocols, new analysis and new modeling methods may need to be developed. Thus, the main contribution of the new findings are the new questions which open the path to numerous branches of original research - future work.

6 Conclusion

The conclusion is bold: stress-space solutions could be incompatible with the properties governing disturbed sand stiffness behavior. Disturbed sand stiffness behaves as a function of strain (deformation), rather than stress (force). $U(F)$ models may be inadequate for $F(U)$ problems. Alas, a potentially compatible (strain-space plasticity) formulation already exists [22]. It is rarely encountered in geotechnics, but is used in neighboring branches of material science [7], [15]. In addition to being an $F(U)$ model (thus, likely compatible with $F(U)$ problems), strain-space plasticity offers substantial computation benefits: fewer matrix inversions, fewer return mapping iterations.

The conclusion was reached in the outcome of trying a novel analysis method. The guessing game. The original, non-geotechnical perspective analyses the data structure governing the problem (stiffness) itself. Rather than anchoring to pre-existing convention, the guessing game forces to reformulate the problem, and approach it from a different perspective: analyzing disturbed sand as a finite-state transition system. This unconventional methodology has revealed principles which allow to control both loss and recovery of stiffness in real-life, real-time testing. The proof is demonstrated empirically. All $Umob$ share the same $Fmob$ limits, but $Fmob$ limits do not produce unique $Umob$ amplitudes (with the exception of converging towards the minimum amplitude). "We can always map from displacement to load, but not from load to displacement" - David Muir Wood lecture, 2015.

The new found requirements could be ignored when dealing with conventional geotechnical problems, where load s are static. Alas, to solve problems containing dynamic loading, a static equilibrium is not enough - the whole equa-

tion of motion has to be accounted for. Not only K is nonlinear, but the C and M components have nonlinear state dependencies. The new findings provide practical means to isolate quasi static K curves and to observe its dependencies by manipulating $Umob$ amplitude and the rate of deformation $\frac{\delta U}{\delta t}$. This allowed to switch the $C \cdot \frac{\delta U}{\delta t}$ component on and off selectively. Thus, the approach might allowing to decipher the full equation of motion - one nonlinear state / phase dependency at a time.

Finally, it is crucial to recognize that the proof is demonstrated ir real-life experiment. A stiffness path equivalent to initial stiffness path was disturbed and recovered at least 5 times in one loading history. Thus, conclusively demonstrating the descriptive, predictive and prescriptive analytic powers delivered by the novel approach.

References

[1] A. Bird. Thomas kuhn. In E. N. Zalta, editor, *The Stanford Encyclopedia of Philosophy*. Fall 2013 edition, 2013.

[2] M. Budhu. Soil mechanics and foundations, (with cd). 2008.

[3] M. Damgaard, L. Andersen, L. Ibsen, H. Toft, and J. Srensen. A probabilistic analysis of the dynamic response of monopile foundations: Soil variability and its consequences. *Probabilistic Engineering Mechanics*, 41:4659, 2015.

[4] C. G. Di Prisco and D. M. Wood. *Mechanical Behaviour of Soils Under Environmentallly-Induced Cyclic Loads*, volume 534. Springer Science & Business Media, 2012.

[5] R. Dobry and T. Abdoun. An investigation into why liquefaction charts work: A necessary step toward integrating the states of art and practice. In *Proc., 5th Int. Conf. on Earthquake Geotechnical Engineering*, pages 13–44. Chilean Geotechnical Society Santiago, Chile, 2011.

[6] R. Dobry and T. Abdoun. Cyclic shear strain needed for liquefaction triggering and assessment of overburden pressure factor k σ. *Journal of Geotechnical and Geoenvironmental Engineering*, page 04015047, 2015.

[7] A. M. Farahat, M. Kawakami, and M. Ohtsu. Strain-space plasticity model for the compressive hardening-softening behaviour of concrete. *Construction and Building Materials*, 9(1):45 – 59, 1995.

[8] L. Ibsen. *The Static and Dynamic Strength of Sand*. Geotechnical Engineering Group, 1995. PDF for print: 11 pp. Published in: Proceedings of the Eleventh European Conference on Soil Mechanics and Foundation Engineering, Copenhagen, 1995 : XI ECSMFE : DGF-bulletin 11, Vol. 6, pp. 69-76.

[9] B. S. Knudsen, M. U. Østergaard, and L. B. Ibsen. Small-scale testing of bucket foundations in sand. Technical report, Department of Civil Engineering, Aalborg University, 2013.

[10] J. Moust. *A new triaxial apparatus*, volume 27. Copenhagen, Geoteknisk Institut, 1970.

[11] S. Nielsen and L. Ibsen. The offshore bucket trail installation. 2015.

[12] S. Nielsen, L. Ibsen, and S. Gres. Cost-effective mass production of mono bucket foundations. 2015. PO: 242.

[13] S. Nielsen, L. Ibsen, and B. Nielsen. *Dynamic behaviour of mono bucket foundations subjected to combined transient loading*, volume 1, pages 313–318. C R C Press LLC, 2015. 978-1-138-02848-7 (set of two volumes hardback + CD-Rom) 978-1-138-02850-0 (Volume1+ CD-Rom) 978-1-138-02852-4 (Volume 2) 978-1-315-67551-0 (ebook PDF).

[14] S. D. Nielsen. *Transient monotonic and cyclic load effects on mono bucket foundations*. PhD thesis, Aalborg Universitetsforlag, 2016.

[15] P. Pankaj and F. E. Donaldson. Algorithms for a strain-based plasticity criterion for bone. *International journal for numerical methods in biomedical engineering*, 29(1):40–61, 2013.

[16] T. Sabaliauskas, A. T. Diaz, L. B. Ibsen, and S. D. Nielsen. Observations during static and cyclic undrained loading of dense aalborg university sand no. 1. Technical report, Aalborg University, DCE Technical Memorandum, 2014.

[17] T. Sabaliauskas and L. Ibsen. *Cyclic Triaxial Loading of Cohesionless Silty Sand*, pages 821–826. International Society of Offshore and Polar Engineers, 2015.

[18] T. Sabaliauskas, L. B. Ibsen, et al. Triaxial testing beyond yielding. In *The 27th International Ocean and Polar Engineering Conference*. International Society of Offshore and Polar Engineers, 2017.

[19] A. N. Schofield. *Disturbed soil properties and geotechnical design*. Thomas Telford, 2005.

[20] I. Stroescu and P. Frigaard. *Scour properties of mono bucket foundation*, pages 335–341. C R C Press LLC, 2016.

[21] D. M. Wood. *Geotechnical modelling*, volume 1. CRC Press, 2003.

[22] P. J. Yoder. A strain-space plasticity theory and numerical implementation. (EERL 80-07), August 1980. A Report on Research Concluded Under Grants from National Science Foundation.

[23] J.-H. S. Yun Wook Choo, Tae-Woo Kang. Centrifuge study on undrained and drained behaviors of a laterally loaded bucket foundation in a silty sand. In *Proceedings of the Twenty-fifth (2015) International Ocean and Polar Engineering Conference*. International Society of Offshore and Polar Engineers (ISOPE), 2015. PO: 963.

ISSN 1901-726X
DCE Technical Report No. 249